Synthesis and spectroscopic characterization of alkali-metal intercalated $ZrSe_2$ †

Konstantin Nikonov,*[a] Niels Ehlen,[a‡], Boris Senkovskiy[a], Nihit Saigal[a], Alexander Fedorov[a], Alexei Nefedov[b], Christoph Wöll[b], Giovanni di Santo[c], Luca Petaccia[c] and Alexander Grüneis*[a]

We report on the synthesis and spectroscopic characterization of alkali metal intercalated $ZrSe_2$ single crystals. $ZrSe_2$ is produced by chemical vapour transport and then Li intercalated. Intercalation is performed from the liquid phase (via butyllithium) and from the vapour phase. Raman spectroscopy of intercalated $ZrSe_2$ reveals phonon energy shifts of the Raman active A_{1g} ad E_g phonon modes, the disappearance of two-phonon modes and new low wavenumber Raman modes. Angle-resolved photoemission spectroscopy is used to perform a mapping of the Fermi surface revealing an electron concentration of 4.7×10^{14} cm^{-2}. We also perform vapour phase intercalation of K and Cs into $ZrSe_2$ and observe similar changes in the Raman modes as for the Li case.

1 Introduction

Intercalation chemistry between a wide range of host materials and intercalant species allows one to engineer the physical properties of layered materials. Perhaps the best-studied example of this kind are the graphite intercalation compounds [1]. For alkali and alkali-earth metal intercalants, the intercalant atom acts as a charge dopant and graphite becomes superconducting [2–4]. Intercalation of related layered materials such as boron nitride [5], transition metal dichalcogenides (TMDCs) [6,7] and black phosphorous [8,9] has also been performed. The largest number of possible combinations between host and intercalant exists for TMDCs which come in the largest variety of host structures [10]. Some of the TMDCs like $ZrSe_2$ are interesting materials for thermoelectric application. In particular, it has been shown that doping can be used to engineer the optimal Seebeck coefficient for a given temperature [11].Our experiments have also revealed that the structural quality of $ZrSe_2$ remains intact after intercalation of alkali metals which allows performing a comparative study.

Regarding the intercalation, we have to distinguish 1) vapour and liquid phase phase intercalation, 2) electrochemical intercalation and 3) liquid ammonia assisted intercalation. Vapour phase intercalation can be performed in an ampoule or by evaporating the alkali metal onto the surface of the host crystal. The latter is especially used in surface science experiments such as photoemission. The butyl-alkali intercalation method is based on inter-

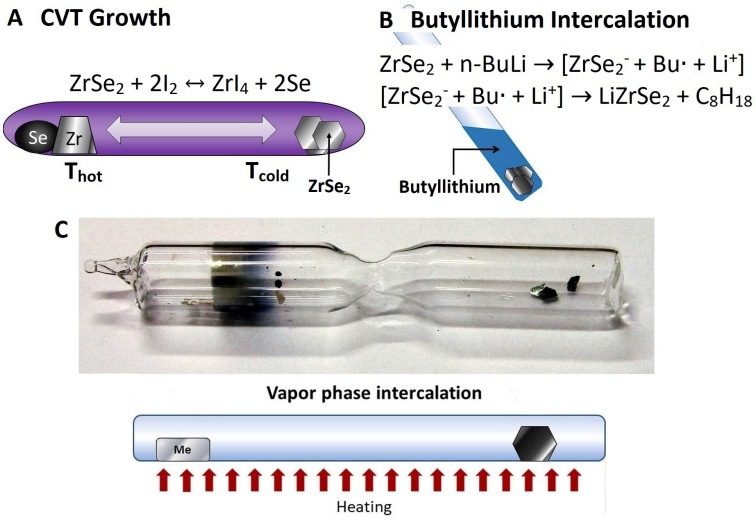

Fig. 1 A) Schematics of the growth of $ZrSe_2$ single crystals by chemical vapour transport (CVT) reaction. B) butyllithium intercalation. C) Vapour-phase intercalation: photograph and sketch (Me stands for alkali metal).

[a] *II. Physikalisches Institut, Universität zu Köln, Zülpicher Strasse 77, 50937 Köln, Germany. Fax: ++49 221 470 5178; Tel: ++49 221 4703461; E-mail: grueneis@ph2.uni-koeln.de; nikonov@ph2.uni-koeln.de;*

[b] *Institut für Funktionelle Grenzflächen, Karlsruher Institut für Technologie, Eggenstein-Leopoldshafen, Germany*

[c] *Elettra Sincrotrone Trieste, Strada Statale 14 km 163.5, 34149 Trieste, Italy*

action between butyl-alkali, typically butyllithium solution and $ZrSe_2$ crystals immersed into it. At first an electron is transferred to $ZrSe_2$ from Bu^-, forming $ZrSe_2^-$, and Li^+ ion diffuse into layered structure of $ZrSe_2$ to compensate negative charge. Then two butyl radicals combine and form octane, which readily evaporates from the solution.

The main downside of this method is the fact that due to the more unstable nature of other butyl-alkali compounds, only butyllithium solution can be easily acquired and is relatively safe to work with, thus limiting wide usage of this method to Li intercalation only. Electrochemical intercalation can be peformed in an electrochemical cell where alkali metal ions are solved in an electrolyte. This method has been applied for the transition metal dichalcogenides [12]. Ammonia-driven intercalation is based on the unique ability of liquid ammonia to form a stable solution with all alkali metals without chemical interaction. Low temperatures are required to keep ammonia in the liquid phase and also help to control the reaction rate and prevent destruction of crystals during intercalation.

After performing intercalation one wishes to characterize spectroscopically the reaction product, in particular regards to the charge transferred from the intercalant to the host derived electronic system. To that end angle-resolved photoemission (ARPES) is a key technique that allows to directly probe the electron energy band structure. It has yielded e.g. the Fermi level shift of the potassium doped graphite compound with KC_8 stoichiometry [13].

In the present work we prepare and spectroscopically study $ZrSe_2$ alkali metal intercalation compounds [14]. $ZrSe_2$ is a semiconductor of recent interest as it can be grown in high quality on high-k dielectrics and is therefore a good material for field effect transistor applications [15]. ARPES spectroscopy has also revealed that spin-orbit coupling effects in $ZrSe_2$ lead to a valence band splitting of $\sim$300 meV in the valence band at the A point of the 3D Brillouin zone [16]. It has also been shown by ARPES that alkali metal intercalation turns $ZrSe_2$ into a metal both in case of Na [15] and Cs doping [14,17] with similar effects observed for ZrS_2 [18]. However the shape of the Fermi surface has not been shown and the carrier concentration has not been estimated. Raman spectroscopy of doped $ZrSe_2$ revealed shifts of the Raman active phonon modes. However, the low wavenumber (LWN) Raman spectrum of intercalated $ZrSe_2$ has not been studied yet. Little is known regarding the effect of different alkali intercalants. The present work addresses these issues. We prepare bulk Li doped $ZrSe_2$ by butyllithium intercalation for Raman spectroscopy and surface Li doped $ZrSe_2$ by evaporation of Li in ultra-high vacuum conditions for ARPES. Raman spectroscopy reveals phonon shifts upon doping in agreement to previous literature. In addition we observe peculiar low wavenumber (LWN) phonons upon intercalation that have not been reported so far. A mapping of the Fermi surface of Li doped $ZrSe_2$ by ARPES reveals a carrier concentration of 4.7×10^{14} cm^{-2}. Finally, K and Cs intercalation compounds are prepared by vapour phase intercalation and characterized by ultra-high vacuum Raman spectroscopy. For these intercalants, the LWN phonons are shifted in frequency pointing towards a dopant dependent phonon mode.

2 Synthesis

2.1 Synthesis of pristine $ZrSe_2$

Large crystals of $ZrSe_2$ were grown from pure substances by chemical transport reaction method in vapour phase (CVT) [19]. Figure 1A depicts a sketch of the growth procedure. Stoichiometric amounts of metallic Zr (Sigma-Aldrich) and granular Se were sealed in evacuated quartz tube along with a Pyrex capillary containing 0.05g of crystallised iodine as a transporting agent. Sealed ampoule was placed in a two-zone tubular furnace with temperature gradient of 115°C between cold (810°C) and hot (925°C) zones of the furnace and held for 120 hours. Under those conditions gaseous iodides of Zr are formed and transported along the temperature gradient to the cold zone of the furnace. Temperature decreasing shifts chemical balance back to the forming of $ZrSe_2$ which crystallizes in the cold end of the ampoule in form of thin shiny plates. The average crystal size was $\sim$5mm^2. The grown crystals were taken out from the ampoule, washed with distilled water and heated under vacuum to remove excess of selenium and iodine left on the crystal surface. Pristine $ZrSe_2$ crystals are thin gray-colored platelets, hexagonal in shape and possess metallic shine. On the surface of large crystals one may see spiraling growth pattern. X-ray photoemission spectroscopy (XPS) experiments were carried out at HESGM beamline at Helmholtz Zentrum Berlin (HZB) [20]. Figure 2A shows an XPS spectrum measured in the vicinity of the Zr and Se 3d core levels confirming the chemical purity of $ZrSe_2$ single crystals. Figure 2B shows a Laue diffraction pattern confirming a good structural quality of grown $ZrSe_2$ crystals. An overlay with a simulated diffraction pattern suggests an expected 1T-structure (Fig. 2C). We also have carried out x-ray diffraction to determine the lattice parameters as $a = b = 3.765(2)$Angstrom and $c = 6.145(3)$Angstrom.These are in good agreement to the literature [21].

2.1.1 Lithium intercalation

Figure 1B depicts a sketch of Lithium intercalation by the conventional butyllithium method [22]. A $ZrSe_2$ crystal was immersed into 1M n-butyllithium solution in hexane for 72h, washed with hexane and stored under Ar. The intercalated crystal turns blue and its surface begins to degrade. The Li doped crystals undergo deintercalation if exposed to atmosphere.

2.1.2 Vapour phase intercalation

Figure 1C depicts a photograph and a sketch of vapour phase intercalation. Potassium and caesium intercalations were carried out in this way. The alkali metal and $ZrSe_2$ crystals were placed into an evacuated Pyrex ampoule. The ampoule was placed into a thermal gradient of 150-200°C for 96h. Alkali vapor interacts with $ZrSe_2$ and metal atoms diffuse into the layered structure. During this process direct contact of the crystals with molten metal was avoided since high reaction rates affect the crystal quality. The intercalated crystals turn blue and readily deintercalate if exposed to air.

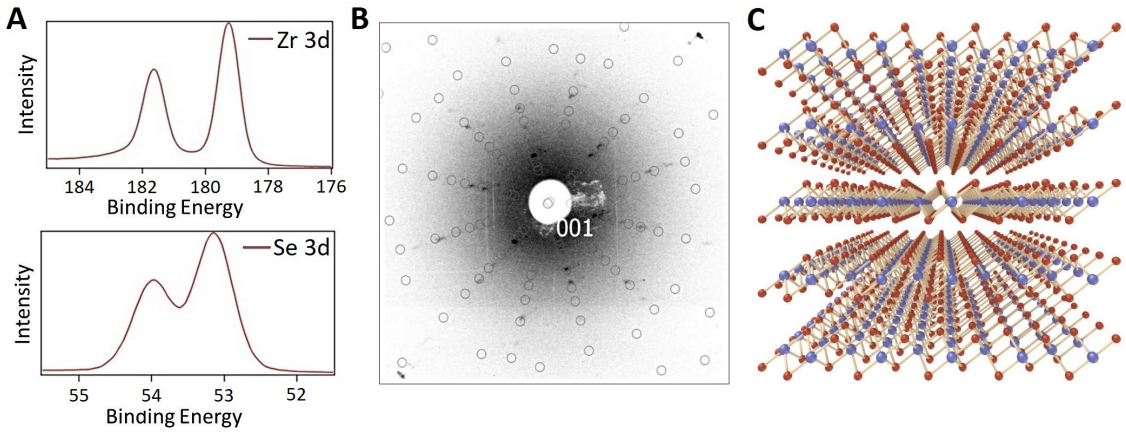

Fig. 2 A) X-ray photoelectron spectroscopy of as-synthesized $ZrSe_2$. The Zr 3d and Se 3d peaks are shown. B) Laue diffraction pattern of as-synthesized $ZrSe_2$. The open circles depict calculations of diffraction spots. C) Sketch of the crystal structure of the 1T phase (Zr in blue, Se in red).

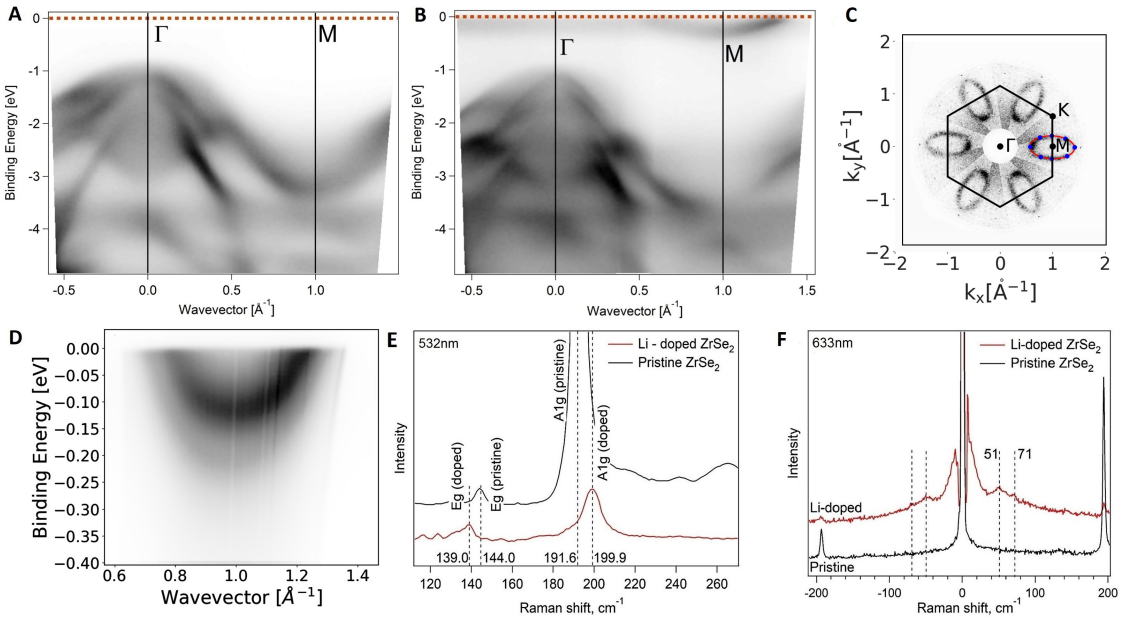

Fig. 3 ARPES ($h\nu = 36$ eV, T=20 K) scan along the high symmetry ΓM line of A) pristine and B) Li-doped $ZrSe_2$. C) Fermi surface mapping (a symmetrization has been applied). The blue points denote the experimental ARPES maxima and the red line an elliptical fit. The area of the ellipse has been used to determine the charge carrier concentration (see text). The photon energy was $h\nu = 36$ eV in all spectra. D) High-resolution ARPES spectra parallel to the ΓM direction showing a splitting in the conduction band. E) Raman spectra of pristine and Li-doped $ZrSe_2$ measured with a green (λ=532 nm) laser. F) Low wavenumber Raman spectra of pristine and Li-doped $ZrSe_2$ (λ=633 nm). All Raman spectra were recorded at room temperature.

2.1.3 Lithium deposition

For the ARPES experiments, several monolayers of lithium were evaporated from a commercial SAES getter source onto the surface of $ZrSe_2$. The doping was performed in an ultra-high vacuum (UHV) chamber in steps up to the maximum Fermi level with the sample at 20 K. The amount of Li was calibrated by a quartz micro balance.

3 Spectroscopic characterization

3.1 Angle-resolved photoemission spectroscopy

Alkali metal doping of $ZrSe_2$ leads to changes in electronic and crystal structure which can be observed using ARPES. ARPES was performed at the BaDElPh beamline[23] of the Elettra synchrotron in Trieste (Italy) with linear s- and p- polarisation at temperatures of 20 K. The crystal surfaces were prepared in-situ in a vacuum better than 5×10^{-11}mbar and at liquid He temperatures by cleaving with a top post inside the analysis chamber. Immediately after the cleave we determined the high-symmetry directions through low-energy electron diffraction. ARPES data taken from pristine $ZrSe_2$ are shown in Figure 3A and reveals a semiconductor band structure with the valence band maximum at the Γ point of the Brillouin zone. Upon doping by Li this picture drastically changes and the Fermi level moves into the previously unoccuppied conduction band. Most importantly, at the M point in the BZ, a parabolic band appears which crosses the Fermi energy. This clearly indicates a transition from semiconducting to metallic electronic properties. In order to estimate the charge carrier density on the $ZrSe_2$ layers, we performed ARPES mapping of the Fermi surface. The Fermi surface map ($h\nu = 36$ eV) is shown in Figure 3C. This photon energy corresponds to the A point of the 3D BZ. A fit of the ARPES maxima using an ellipse allows to calculate the charge carrier density equal to 4.7×10^{14} electrons per square centimeter. Figure 3D depicts a cut through the pocket ($h\nu = 22$ eV). A splitting of the conduction band by about 100 meV can be seen which we tentatively attribute to spin-orbit coupling[16]. Assuming a complete charge transfer for each Li ion, we estimate a stoichiometry of about 1 Li per two unit cells.

3.2 Raman spectroscopy

3.2.1 Butyllithium intercalated $ZrSe_2$

The Raman spectra of pristine $ZrSe_2$ that we obtained under ambient conditions fit the literature data very well[24]. Alkali metal intercalated $ZrSe_2$ can not be measured in ambient conditions because of the high reactivity with air. We have overcome this problem in two ways. One is that we have made use of an ultra-high vacuum (UHV) Raman system[25,26]. Samples were taken from the ampoules and mounted on a wobble stick in a vacuum suitcase inside a glove box. Then, these samples were transferred into the UHV Raman without exposure to air. A second method that is a bit easier to apply works by reloading the intercalated samples into an ampoule with a flat surface (Hilgenberg) inside an Ar box. This ampoule is sealed by wax and transferred out of the Ar box. We have performed Raman spectroscopy of samples prepared in both ways and did not find a difference in the obtained spectra. Figure 3E depicts Raman spectra of pristine and Li doped $ZrSe_2$. Upon doping with alkali metals, the characteristic peaks of A_{1g} ad E_g modes are shifted to lower and higher wavenumbers, respectively. This observation is in good agreement to previous data[27]. In the case of low frequency Raman spectra (Figure 3F) one can see low energy Raman modes at 51 cm^{-1} and 71 cm^{-1} appearing after doping. Interestingly, there are two more weak Raman modes present in pristine $ZrSe_2$ at 240 cm^{-1} and 260 cm^{-1} (Figure 3E). These have been assigned to two-phonon processes[24]. Upon doping we can not observe them any more which points towards a loss of the resonance condition for two phonon scattering upon shifting the Fermi level. Notably, Raman measurements at several spots across the samples revealed that the intercalated samples are homogeneous.

3.2.2 Cs and K intercalated $ZrSe_2$

Along with well-known Li intercalation we performed K and Cs intercalation from the vapour phase into bulk $ZrSe_2$ crystals. These Raman spectra are shown in Figure 4A an display similar effects as in the lithium doping cases, i.e. the shifting of A_{1g} and E_g phonon modes. The phonon energy shift upon doping was extensively investigated for example for graphene[28]. It has been shown for graphene that there are two main contributions: one is the lattice expansion which causes a downshift. The second contribution is the phonon self energy which can change with doping. We speculate that a similar reasoning might be applied for $ZrSe_2$, too. Interestingly, the low-wavenumber Raman modes for Li, K and Cs intercalants appear at different energies. For the K intercalated $ZrSe_2$, we observe them at 38 cm^{-1} and 62 cm^{-1} respectively, and for Cs intercalated $ZrSe_2$ a broad mode around 60 cm^{-1} appears. These modes have not been reported so far and could in principle be a result of one or several following reasons: 1) changes in the lattice structure and defect formation upon interaction with the alkali metal 2) dopant derived vibrations and 3) electronic Raman scattering. The high structural quality of doped samples as e.g. evidenced by ARPES makes 1) unlikely. Moreover, the temperature of the Raman measurements was room temperature which makes 3) unlikely. Since there is a distinct dopant dependence which shifts the phonons to lower wavenumber with increasing dopant mass, we speculate that the LWN phonon modes belong to alkali ion vibrations.

4 Conclusions and outlook

In conclusion we have synthesized Li doped $ZrSe_2$ by butyllithium intercalation from the liquid phase and by evaporation of Li in UHV conditions onto the $ZrSe_2$ surface. For the bulk sensitive Raman spectroscopy, the samples intercalated by butyllithium have been used. For the surface sensitive ARPES method Li evaporation in UHV has been applied. Upon Li doping, the semiconductor $ZrSe_2$ becomes metallic which is evidenced by the appearance of an elliptical Fermi surface around the M point in the 2D BZ. Also the phonon system of $ZrSe_2$ undergoes changes, in particular phonon energy shifts of the Raman active A_{1g} and E_g phonons are observed. We also observe the appearance of new low wavenumber modes in the Raman spectrum whose origin is tentatively attributed to dopant derived vibrations. The connection of these

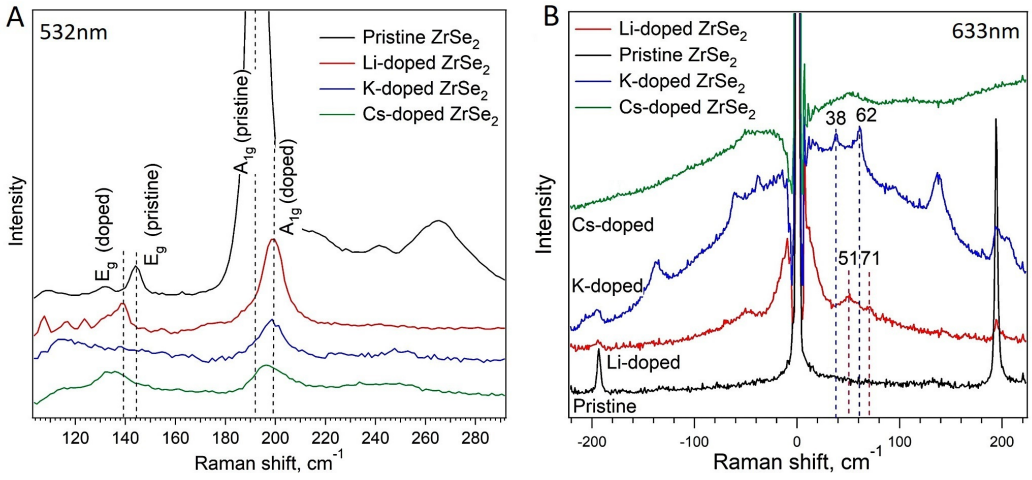

Fig. 4 A) Raman modes of pristine and intercalated (Li, K, Cs) $ZrSe_2$ (λ=532 nm). B) Low-frequency Raman spectrum (λ=633 nm). All Raman spectra were recorded at room temperature.

new modes to the intercalant is corroborated by their appearance for K and Cs intercalants at slightly different frequencies.

Conflict of interest

There are no conflicts to declare.

5 Acknowledgements

K.N., N.E., B.S., A.F. and A.G. acknowledge the ERC grant no. 648589 'SUPER-2D', funding from DFG project CRC 1238 (project A1) and DFG project GR 3708/2-1. The research leading to these results has received funding from the European Community's Horizon 2020 Programme under grant agreement n. 730872 (CALIPSOplus). A.N. and C.W. acknowledge STN programme (Karlsruhe Institute of Technology) for a partial support of these experiments. We thank HZB and Elettra for the allocation of synchrotron radiation beamtimes.

References

1 M. S. Dresselhaus and G. Dresselhaus, *Advances in physics*, 2002, **51**, 1–186.

2 N. B. Hannay, T. H. Geballe, B. T. Matthias, K. Andres, P. Schmidt and D. MacNair, *Phys. Rev. Lett.*, 1965, **14**, 225–226.

3 T. E. Weller, M. Ellerby, S. S. Saxena, R. P. Smith and N. T. Skipper, *Nat. Phys.*, 2005, **1**, 39–41.

4 N. Emery, C. Hérold, M. d'Astuto, V. Garcia, C. Bellin, J. F. Marêché, P. Lagrange and G. Loupias, *Phys. Rev. Lett.*, 2005, **95**, 087003.

5 G. L. Doll, J. S. Speck, G. Dresselhaus, M. S. Dresselhaus, K. Nakamura and S. Tanuma, *Journal of Applied Physics*, 1989, **66**, 2554–2558.

6 J. Wilson, F. D. Salvo and S. Mahajan, *Advances in Physics*, 1975, **24**, 117–201.

7 E. Marseglia, *International Reviews in Physical Chemistry*, 1983, **3**, 177–216.

8 R. Zhang, J. Waters, A. K. Geim and I. V. Grigorieva, *Nature Communications*, 2017, **8**, 15036.

9 G. Abelan, C. Neiss, V. Lloret, S. Wild, J. C. Chacon-Torres, K. Werbach, F. Fedi, H. Shiozawa, A. Goerling, H. Peterlik, T. Pichler, F. Hauke and A. Hirsch, *Angewandte Chemie International Edition*, 2017, **56**, 15267–15273.

10 M. Chhowalla, H. S. Shin, G. Eda, L.-J. Li, K. P. Loh and H. Zhang, *Nat Chem*, 2013, **5**, 263–275.

11 G. Ding, G. Y. Gao, Z. Huang, W. Zhang and K. Yao, *Nanotechnology*, 2016, **27**, 375703.

12 E. Hitz, J. Wan, A. Patel, Y. Xu, L. Meshi, J. Dai, Y. Chen, A. Lu, A. V. Davydov and L. Hu, *ACS Applied Materials & Interfaces*, 2016, **8**, 11390–11395.

13 A. Grüneis, C. Attaccalite, A. Rubio, D. V. Vyalikh, S. L. Molodtsov, J. Fink, R. Follath, W. Eberhardt, B. Büchner and T. Pichler, *Phys. Rev. B*, 2009, **80**, 075431.

14 H. Starnberg, *Acta Physica Polonica A*, 2001, **100**, 301–318.

15 M. J. Mleczko, C. Zhang, H. R. Lee, H.-H. Kuo, B. Magyari-Köpe, R. G. Moore, Z.-X. Shen, I. R. Fisher, Y. Nishi and E. Pop, *Science Advances*, 2017, **3**, year.

16 M. Moustafa, A. Ghafari, A. Paulheima, C. Janowitz and R. Manzkea, *Journal of Electron Spectroscopy and Related Phenomena*, 2013, **189**, 35–39.

17 H. E. Brauer, H. I. Starnberg, L. J. Holleboom and H. P. Hughes, *Journal of Physics: Condensed Matter*, 1995, **6**, 7741–7760.

18 A. Ghafari, C. Janowitz and R. Manzke, *Journal of Physics: Condensed Matter*, 2013, **25**, 315502.

19 H. Schäfer, *Chemische Transportreaktionen*, Verlag Chemie, Weinheim, 1962.

20 A. Nefedov and C. Wöll, *Advanced Applications of NEXAFS Spectroscopy for Functionalized Surfaces. In: Bracco G., Holst B. (eds) Surface Science Techniques.*, Springer, Berlin, Heidelberg, 2013, vol. 51, pp. 277–303.

21 C. R. Whitehouse and A. A. Balchin, *physica status solidi (a)*, 1978, **47**, K173–K176.

22 D. W. Murphy, F. J. D. Salvo, J. George W. Hull and J. V. Waszczak, *Inorganic Chemistry*, 1976, **15**, 17–21.

23 L. Petaccia, P. Vilmercati, S. Gorovikov, M. Barnaba, A. Bianco, D. Cocco, C. Masciovecchio and A. Goldoni, *Nuclear Instruments and Methods in Physics Research Section A: Accelerators, Spectrometers, Detectors and Associated Equipment*, 2009, **606**, 780–784.

24 S. Manas-Valero, V. Garcia-Lopez, K. C. Andres and M. Galbiati, *Applied sciences*, 2016, **6**, year.

25 B. V. Senkovskiy, A. V. Fedorov, D. Haberer, M. Farjam, K. A. Simonov, A. B. Preobrajenski, N. Martensson, N. Atodiresei, V. Caciuc, S. Blügel, A. Rosch, N. I. Verbitskiy, M. Hell, D. V. Evtushinsky, R. German, T. Marangoni, P. H. M. van Loosdrecht, F. R. Fischer and A. Grüneis, *Advanced Electronic Materials*, 2017, 1600490.

26 A. Grüneis, B. Senkovskiy, A. Fedorov, M. Hell and S. Michel, *Encyclopedia of surface science*, 2017, **at press**, year.

27 P. C. Klipstein, C. M. Pereira and R. H. Friend, *Philosophical Magazine Part B*, 1987, **56**, 531–539.

28 M. Lazzeri and F. Mauri, *Phys. Rev. Lett.*, 2006, **97**, 266407.